We are IntechOpen, the world's leading publisher of Open Access books Built by scientists, for scientists

4,800
Open access books available

122,000
International authors and editors

135M
Downloads

Our authors are among the

154
Countries delivered to

TOP 1%
most cited scientists

12.2%
Contributors from top 500 universities

CLARIVATE ANALYTICS BOOK CITATION INDEX INDEXED

WEB OF SCIENCE™

Selection of our books indexed in the Book Citation Index in Web of Science™ Core Collection (BKCI)

Interested in publishing with us?
Contact book.department@intechopen.com

Numbers displayed above are based on latest data collected.
For more information visit www.intechopen.com

4

Pure $\chi^{(3)}$ Third-Harmonic Generation in Noncentrosymmetric Media

Kentaro Miyata
Chitose Institute of Science and Technology
Japan

1. Introduction

Recently, higher-order nonlinear effects have attracted great attention with the development of ultrafast laser technology. Using high peak-power lasers, phase-matched third-harmonic generation (THG) ($\omega + \omega + \omega \rightarrow 3\omega$) has been demonstrated in solids to directly obtain frequency-tripled output of the fundamental light in a simple way. The beginning of THG experiments using crystals was as early as 1960s. In this early stage of THG experiments, the centrosymmetric $CaCO_3$, calcite, was investigated by using a Q-switched ruby laser (Terhune et al., 1962, 1963).

Thanks to the invention of the mode-lock technique, ultrashort-pulse lasers became available, which made it possible to obtain stronger nonlinear interaction in crystals without laser-induced damage, since the damage threshold of materials increases as the laser pulse duration becomes short. With a mode-locked Nd-doped laser, Akhmanov et al. achieved phase-matched interactions for forth-harmonic generation (FHG) in $LiCOOH \cdot H_2O$ (Akhmanov et al., 1974) and fifth-harmonic generation in calcite (Akhmanov et al., 1975). Comparing the determined nonlinear susceptibilities relative to those for the lower-order ones, they have shown that electric susceptibilities for the higher-order processes decrease more rapidly with increasing the nonlinear order. In these works, the cascade processes of the lower-order nonlinearities in higher-harmonics generation were discussed in detail.

In addition, materials having large nonlinear electric susceptibilities have been developed for noncentrosymmetric crystals. Okada (1971) observed phase-matched THG of a Q-switched Nd:YAG laser in $LiIO_3$, reporting the effective third-order susceptibilities that are two orders of magnitude larger than those for KDP and ADP. The first observations of phase-matched THG (Chemla et al., 1974) and FHG (Kildal et al., 1979) in the transparent mid-IR region were made in $CdGeAs_2$ by using a CO_2 laser at 10.6 μm, where the effective third-order and fourth-order nonlinearities determined from the harmonic signals were compared with the theoretical estimates of the pure $\chi^{(3)}$ and $\chi^{(4)}$ components, respectively. Efficient THG was expected to be obtained from the determined $\chi^{(3)}$ while the large discrepancy encountered for the magnitudes of $\chi^{(4)}$ indicated the significant contribution from the cascade processes.

Finally, conversion efficiencies for THG in solids reached ~1% with the most widely used nonlinear crystals, β-BaB_2O_4 (BBO) and $KTiOPO_4$ (KTP). Qiu and Penzkofer (1988) attained a conversion efficiency of 0.8% in BBO for THG of a Nd:glass laser with a pulse duration of 5 ps, for which the crystal was irradiated by the intensity of 50 GW/cm². It was found that

Source: Advances in Lasers and Electro Optics, Book edited by: Nelson Costa and Adolfo Cartaxo,
ISBN 978-953-307-088-9, pp. 838, April 2010, INTECH, Croatia, downloaded from SCIYO.COM

compared with calcite (Penzkofer et al., 1988), this material possesses ~40 times larger effective nonlinearity with smaller walk-off and larger angular acceptance, indicating the superior properties for this application. With a chirped pulse amplification of the Nd:glass laser, Banks et al. (1999) have attempted to use higher pulse intensity with shorter pulse duration in BBO, taking into account the increase of the damage threshold. Focusing the 350-fs-pulse beam into the nonlinear crystal resulted in a highest conversion efficiency of ~6% for third-order frequency conversions in crystals, where the intensity of the fundamental beam was as high as ~200 GW/cm^2. In addition, they have succeeded to distinguish the cascade process from the direct process through the azimuth angle dependence of the output signals, and concluded that the contributions from the cascade processes to the phase-matched THG are significant in the overall conversion efficiencies (Banks et al., 2002).

The large third-harmonic (TH) conversion efficiencies in KTP have been achieved by two different groups, using tunable picosecond optical parametric systems. Boulanger and co-workers (Feve et al., 2002) produced the angularly noncritical phase-matched THG of 1.618 μm radiation with 2.4% efficiency while under the phase-matching condition for sum-frequency generation (SFG) ($\omega + 2\omega \rightarrow 3\omega$) in the similar spectral range, Takagi and Muraki (2000) have achieved a single-crystal TH efficiency of 5% that was five times larger than the phase-matched THG observed with the same fundamental source. According to the work of Boulanger et al (1999), the contribution from the cascade processes to phase-matched THG in KTP is much smaller compared to direct process. Recently, to completely eliminate the involved cascade process for the future quantum correlation experiment based on the three-photon downconversion, the same group used the centrosymmetric TiO_2 rutile for the single-crystal THG, demonstrating a significant enhancement of the cubic TH efficiency at the week input-power level (Gravier & Boulanger, 2006, 2007).

In this study, phase-matched THG in noncentrosymmetric media have been further investigated by using BiB_3O_6 (BIBO) (Miyata et al., 2008, 2009). The symmetry and birefringence analysis has revealed the existence of the phase-matching condition for the direct cubic process, where the cascading quadratic processes are precluded by zero effective nonlinearity. To understand the proposed pure cubic process, Section 2 discusses the cascade process that is generally involved in THG of noncentrosymmetric crystals. The next section presents the third-order frequency conversions in BIBO, including the first realized pure $\chi^{(3)}$ THG in such media. The discussion is separately given in Section 4 to generalize the present result to other materials. Finally, Section 5 concludes this chapter.

2. Cascade third-harmonic generation

In general, frequency tripling of a laser is carried out with two nonlinear crystals both under the phase-matching conditions. First crystal is used for generating the second harmonic (SH) of the fundamental source, and the second crystal is used for mixing the SH with the residual fundamental to create its TH. Since these crystals can be independently adjusted in the system, phase-matching conditions for the second-harmonic generation (SHG) and SFG processes are easily achieved by the angle or temperature tuning at the given fundamental wavelength. This two-step process, $\chi^{(2)}(3\omega, \omega, 2\omega):\chi^{(2)}(2\omega, \omega, \omega)$, exists also for THG observed in a single nonlinear crystal and occurs simultaneously with the direct third-order process mediated by the pure cubic nonlinearity $\chi^{(3)}(3\omega, \omega, \omega, \omega)$. Its phase-matching condition is identical with that for the direct THG as a whole and given by

$$\Delta k_{\mathrm{THG}} = \Delta k_{\mathrm{SHG}} + \Delta k_{\mathrm{SFG}} \tag{1}$$

where $\Delta k_{\mathrm{THG}} = k_{1a} + k_{1b} + k_{1c} - k_3$, $\Delta k_{\mathrm{SHG}} = k_{1a} + k_{1b} - k_2$, and $\Delta k_{\mathrm{SFG}} = k_{1c} + k_2 - k_3$. Thus, when the phase-matching condition for the overall process is fulfilled (i.e. $\Delta k_{\mathrm{THG}} = 0$), the individual SHG and SFG processes are generally not phase-matched inside the nonlinear crystal. Under this condition, the direct third-order and cascading second-order processes have the same order of magnitude and mutually interferes in a constructive or destructive way, provided the effective second-order nonlinearity is nonzero. Also under the phase-matching conditions for either SHG or SFG process, the same order of magnitude of THG becomes feasible. However, in this case, the contribution of the pure cubic nonlinearity to THG is negligibly small because the phase-matching conditions for THG are not fulfilled inside the nonlinear crystal.

Since our interest in the present study is the nonlinear interactions via cubic nonlinearity, consider the specific case, $\Delta k_{\mathrm{THG}} \to 0$, and equivalently, $\Delta k_{\mathrm{SHG}} \sim -\Delta k_{\mathrm{SFG}}$, for the THG process. Solving the nonlinear wave equations that are coupled among the fundamental, SH, and TH waves, under the slowly varying amplitude and fixed-field approximations, the overall TH conversion efficiency is found to be proportional to the square of phase-matching factor

$$\mathrm{sinc}\left(\frac{\Delta k_{\mathrm{THG}}\,\ell}{2}\right) \tag{2}$$

and effective nonlinear constant

$$c_{\mathrm{eff}} = c_{\mathrm{eff}}^{(3)} + \sum_{\mathrm{i}} c_{\mathrm{i,eff}}^{(2)} \tag{3}$$

with

$$c_{i,\mathrm{eff}}^{(2)} = \frac{D_{\mathrm{i}}^{(2)}}{D^{(3)}}\left(\frac{2\omega\, d_{\mathrm{i,eff}}^{\mathrm{SHG}}\, d_{\mathrm{i,eff}}^{\mathrm{SFG}}}{c n_{\mathrm{i},2\omega}\Delta k_{\mathrm{i,SHG}}}\right) \tag{4}$$

where ℓ is the crystal length and ω is the fundamental wavelength. The first term of Eq. (3) is the effective nonlinear constant calculated by third-order susceptibilities, and the second term is the sum of the cascading contributions calculated by Eq. (4), where $D^{(2)}$ and $D^{(3)}$ represent the degeneracy factors for SHG and THG, respectively, i.e. $D^{(2)} = 1$ or 2, and $D^{(3)} = 1$ or 3 for parallel or orthogonal polarization configuration of the fundamental, respectively. The d_{eff} is the effective second-order nonlinear constants at the given fundamental propagation direction. The subscript i indicates the cascade processes listed in Table 1, where the two eigenmodes for refractive indices n_s and n_f are defined as $n_s > n_f$ for the slow and fast waves, respectively. The typical value of $c_{\mathrm{eff}}^{(2)}$ with $d_{\mathrm{eff}} \neq 0$ and $\Delta k \neq 0$ are calculated to be in the range of 10^{-22}–10^{-24} m^2/V^2 for oxide materials, which is almost same order of magnitude as that of $c_{\mathrm{eff}}^{(3)}$.

3. Third-order frequency conversions in BIBO

3.1 Effective nonlinear constants

Because of the lack of inversion symmetry, third-order frequency conversions in BIBO are also accompanied by cascading quadratic processes. To estimate the magnitude of those

Direct process		Cascade process		
Type	THG	i	SHG	SFG
1	$s_1 + s_1 + s_1 \rightarrow f_3$	1	$s_1 + s_1 \rightarrow s_2$	$s_1 + s_2 \rightarrow f_3$
		2	$s_1 + s_1 \rightarrow f_2$	$s_1 + f_2 \rightarrow f_3$
2	$f_1 + s_1 + s_1 \rightarrow f_3$	1	$s_1 + s_1 \rightarrow s_2$	$f_1 + s_2 \rightarrow f_3$
		2	$s_1 + s_1 \rightarrow f_2$	$f_1 + f_2 \rightarrow f_3$
		3	$f_1 + s_1 \rightarrow s_2$	$s_1 + s_2 \rightarrow f_3$
		4	$f_1 + s_1 \rightarrow f_2$	$s_1 + f_2 \rightarrow f_3$
3	$f_1 + f_1 + s_1 \rightarrow f_3$	1	$f_1 + s_1 \rightarrow s_2$	$f_1 + s_2 \rightarrow f_3$
		2	$f_1 + s_1 \rightarrow f_2$	$f_1 + f_2 \rightarrow f_3$
		3	$f_1 + f_1 \rightarrow s_2$	$s_1 + s_2 \rightarrow f_3$
		4	$f_1 + f_1 \rightarrow f_2$	$s_1 + f_2 \rightarrow f_3$

Table 1. Cascade process coupled with the direct type-1, type-2, and type-3 THG processes. The subscripts 1, 2, and 3 denote the fundamental, SH, and TH waves, respectively. The order of i is arbitrary.

processes in this noncentrosymmetric crystal, we first derive the effective second-order nonlinear constants.

The BIBO belongs to the monoclinic system with point symmetry 2, and the principal optical axis x ($n_x < n_y < n_z$) coincides with the crystallographic two-fold rotation axis b (Hellwig et al., 2000). Here, the tensor elements for the second-order susceptibilities $\chi_{ijk}(\omega_1 + \omega_2, \omega_1, \omega_2)$ are expressed with the optical coordinate system xyz for convenient use in the frequency conversion experiments, i.e. each subscript i, j, and k is defined to take the value, 1 = x, 2 = y, or 3 = z. Applying the symmetry operation of the two-fold rotation axis and using a contracted notation for the last two indices, i.e. l = (1, 2, 3, 4, 5, 6) = (xx, yy, zz, yz, zx, xy), the zero and nonzero tensor elements for second-order nonlinear constants ($d_{ijk} = 1/2\chi_{ijk}$) of BIBO are determined as follows:

$$d_{il} = \begin{pmatrix} d_{11} & d_{12} & d_{13} & d_{14} & 0 & 0 \\ 0 & 0 & 0 & 0 & d_{25} & d_{26} \\ 0 & 0 & 0 & 0 & d_{35} & d_{36} \end{pmatrix} \tag{5}$$

When the Kleinman symmetry is applied, $d_{12} = d_{26}$, $d_{13} = d_{35}$, and $d_{14} = d_{25} = d_{36}$ hold in the above expressions. The number of independent coefficients is, therefore, reduced from 8 to 4. Note that although Kleinman symmetry is sometimes reported to be violated in crystals, this symmetry becomes an excellent approximation in the transparent range.

The absolute values and relative signs of the nonzero second-order nonlinear constants for BIBO have been investigated by Hellwig et al. (1999, 2000) with a Maker fringe method using a quasi-cw Nd:YAP laser at 1.0795 μm. Since each tensor element presented in their work is represented by the crystallophysical system XYZ, the transformation of these tensors to the optical coordinate system xyz is required with the consideration of orientation of the principal optical axes (Hellwing et al., 2000). For instance, the corrected results for SHG of the 1.0795 μm radiation at 20°C in the xyz frame are listed in Table 2.

d_{il} (pm/V)		d_{il} (pm/V)	
d_{11}	± 2.54	d_{25}	± 1.70
d_{12}	± 2.95	d_{26}	± 3.49
d_{13}	∓ 1.94	d_{35}	∓ 1.58
d_{14}	± 1.64	d_{36}	± 1.73

Table 2. Second-order nonlinear constants of BIBO for SHG of the 1.0795 μm radiation in the optical coordinate system *xyz*.

To obtain the effective nonlinear constant d_{eff} for the given propagation direction, the projection of light polarization vectors to the independent nonlinear constants d_{il} has to be first performed. Then, multiplying d_{il} with the determined electric-field components, the effective nonlinear constants are calculated for each interaction type. For biaxial crystals, their analytical forms for arbitrary propagation directions are always complicated without approximations, but simplified by restricting the propagation directions in the principal planes. When Klienman symmetry and no spatial walk-off approximations are applied to this case, $d_{\text{eff}}(\omega_3^f = \omega_1^s + \omega_2^s) = d_{\text{eff}}(\omega_3^s = \omega_1^s + \omega_2^f) = d_{\text{eff}}(\omega_3^s = \omega_1^f + \omega_2^s)$ and $d_{\text{eff}}(\omega_3^f = \omega_1^s + \omega_2^f) = d_{\text{eff}}(\omega_3^f = \omega_1^f + \omega_2^s) = d_{\text{eff}}(\omega_3^s = \omega_1^f + \omega_2^s)$ hold at the given propagation direction, i.e. the permutation of polarizations becomes possible. Finally, introducing the notations *o* and *e* for the interacting waves with polarizations normal and parallel to the principal plane, respectively, the expressions for effective nonlinear constants of BIBO are reduced as

$$\begin{aligned} d_{\text{eff}}^{sss}(=d_{\text{eff}}^{ooo}) &= 0 \\ d_{\text{eff}}^{ssf}(=d_{\text{eff}}^{ooe}) &= d_{13}\sin\phi \\ d_{\text{eff}}^{sff}(=d_{\text{eff}}^{oee}) &= d_{14}\sin 2\phi \\ d_{\text{eff}}^{fff}(=d_{\text{eff}}^{eee}) &= (d_{11}\sin^2\phi + 3d_{12}\cos^2\phi)\sin\phi \end{aligned} \tag{6-1}$$

in the *xy* plane,

$$\begin{aligned} d_{\text{eff}}^{sss}(=d_{\text{eff}}^{eee}) &= 0 \\ d_{\text{eff}}^{ssf}(=d_{\text{eff}}^{eeo}) &= \pm d_{13}\sin^2\theta \pm d_{12}\cos^2\theta - d_{14}\sin 2\theta \\ d_{\text{eff}}^{sff}(=d_{\text{eff}}^{eoo}) &= 0 \\ d_{\text{eff}}^{fff}(=d_{\text{eff}}^{ooo}) &= \pm d_{11} \end{aligned} \tag{6-2}$$

in the *yz* plane ($\phi = \pm 90°$),

$$\begin{aligned} d_{\text{eff}}^{sss}(=d_{\text{eff}}^{ooo}) &= 0 \\ d_{\text{eff}}^{ssf}(=d_{\text{eff}}^{ooe}) &= d_{12}\cos\theta \\ d_{\text{eff}}^{sff}(=d_{\text{eff}}^{oee}) &= -/+ d_{14}\sin 2\theta \\ d_{\text{eff}}^{fff}(=d_{\text{eff}}^{eee}) &= (d_{11}\cos^2\theta + 3d_{13}\sin^2\theta)\cos\theta \end{aligned} \tag{6-2}$$

in the *zx* plane for ($\phi = 0°/180°$, $0° \le \theta < \Omega_z$ or $180° - \Omega_z < \theta \le 180°$), and

$$\begin{aligned} d_{\text{eff}}^{sss}(=d_{\text{eff}}^{eee}) &= +/-(d_{11}\cos^2\theta + 3d_{13}\sin^2\theta)\cos\theta \\ d_{\text{eff}}^{ssf}(=d_{\text{eff}}^{eeo}) &= d_{14}\sin 2\theta \\ d_{\text{eff}}^{sff}(=d_{\text{eff}}^{eoo}) &= +/- d_{12}\cos\theta \\ d_{\text{eff}}^{fff}(=d_{\text{eff}}^{ooo}) &= 0 \end{aligned} \tag{6-4}$$

in the *zx* plane for (ϕ = 0°/180°, $\Omega_z < \theta < 180° - \Omega_z$), where θ is the polar angle referring to *z* in the range of 0° ≤ θ ≤ 180° and ϕ is the azimuth angle referring to *x* in the range of −180° ≤ ϕ ≤ 180°. The general forms for the type-1 and type-2 interactions outside the principal planes have been obtained by Tzankov and Petrov (2005) by neglecting the dispersion of optic axis angles. Note that the signs of the above equations are in an opposite relation with respect to those given by them, owing to the different definition of the electric polarization state.

Similarly, apart from the cascading effects of the second-order processes given in the preceding, the effective nonlinearity for the third-order frequency conversion is directly determined from the third-order nonlinear susceptibilities χ_{ijkl} ($\omega_1 + \omega_2 + \omega_3$; ω_1, ω_2, ω_3), where each subscripts i, j, and k is defined to take the value, 1 = *x*, 2 = *y*, or 3 = *z*. The zero and nonzero tensor elements for the third-order nonlinear constants (c_{ijkl} =1/4χ_{ijkl}) of BIBO, with a contracted notation, m = (1, 2, 3, 4, 5, 6, 7, 8, 9, 0) = (*xxx*, *yyy*, *zzz*, *yzz*, *yyz*, *xzz*, *xxz*, *xyy*, *xxy*, *xyz*), is given by

$$c_{im} = \begin{pmatrix} c_{11} & 0 & 0 & 0 & 0 & c_{16} & 0 & c_{18} & 0 & c_{10} \\ 0 & c_{22} & c_{23} & c_{24} & c_{25} & 0 & c_{27} & 0 & c_{29} & 0 \\ 0 & c_{32} & c_{33} & c_{34} & c_{35} & 0 & c_{37} & 0 & c_{39} & 0 \end{pmatrix}, \tag{7}$$

indicating the nonzero 9 and 16 elements with and without Klienman symmetry condition, respectively (i.e. $c_{16} = c_{37}$, $c_{18} = c_{29}$, $c_{10} = c_{27} = c_{39}$, $c_{23} = c_{34}$, $c_{24} = c_{35}$, $c_{25} = c_{32}$ under the Klienman symmetry condition). From the reported nonlinear refractive indices (Miller et al., 2008), these values are expected to be larger than those of BBO and is comparable to those of KTP and $LiNbO_3$.

Again, with Klienman symmetry and no spatial walk-off approximations, the corresponding effective nonlinear constants in the principal plane of BIBO are given by

$$\begin{aligned}
&c_{\text{eff}}^{ssss} (= c_{\text{eff}}^{oooo}) = c_{33} \\
&c_{\text{eff}}^{sssf} (= c_{\text{eff}}^{oooe}) = c_{23} \cos\phi \\
&c_{\text{eff}}^{ssff} (= c_{\text{eff}}^{ooee}) = c_{16} \sin^2\phi + c_{24} \cos^2\phi \\
&c_{\text{eff}}^{sfff} (= c_{\text{eff}}^{oeee}) = (c_{25} \cos^2\phi + 3c_{10} \sin^2\phi) \cos\phi \\
&c_{\text{eff}}^{ffff} (= c_{\text{eff}}^{eeee}) = c_{11} \sin^4\phi + c_{22} \cos^4\phi + \frac{3}{2} c_{18} \sin^2 2\phi
\end{aligned} \tag{8-1}$$

in the *xy* plane,

$$\begin{aligned}
&c_{\text{eff}}^{ssss} (= c_{\text{eff}}^{eeee}) = c_{22} \cos^4\theta + c_{33} \sin^4\theta + \frac{3}{2} c_{24} \sin^2 2\theta \\
&\qquad \mp 2(c_{23} \sin^2\theta + c_{25} \cos^2\theta) \sin 2\theta \\
&c_{\text{eff}}^{sssf} (= c_{\text{eff}}^{eeeo}) = 0 \\
&c_{\text{eff}}^{ssff} (= c_{\text{eff}}^{eeoo}) = c_{16} \sin^2\theta + c_{18} \cos^2\theta \mp c_{10} \sin 2\theta \\
&c_{\text{eff}}^{sfff} (= c_{\text{eff}}^{eooo}) = 0 \\
&c_{\text{eff}}^{ffff} (= c_{\text{eff}}^{oooo}) = c_{11}
\end{aligned} \tag{8-2}$$

in the *yz* plane (ϕ = ±90°),

$$
\begin{aligned}
c_{\text{eff}}^{ssss}\,(=c_{\text{eff}}^{oooo}) &= c_{22} \\
c_{\text{eff}}^{sssf}\,(=c_{\text{eff}}^{oooe}) &= -/+c_{25}\sin\theta \\
c_{\text{eff}}^{ssff}\,(=c_{\text{eff}}^{ooee}) &= c_{24}\sin^2\theta + c_{18}\cos^2\theta \\
c_{\text{eff}}^{sfff}\,(=c_{\text{eff}}^{oeee}) &= -/+(c_{23}\sin^2\theta + 3c_{10}\cos^2\theta)\sin\theta \\
c_{\text{eff}}^{ffff}\,(=c_{\text{eff}}^{eeee}) &= c_{11}\cos^4\theta + c_{33}\sin^4\theta + \frac{3}{2}c_{16}\sin^2 2\theta
\end{aligned}
\tag{8-3}
$$

in the zx plane ($\phi = 0°/180°$, $0° \le \theta < \Omega_z$ or $180° - \Omega_z < \theta \le 180°$), and

$$
\begin{aligned}
c_{\text{eff}}^{ssss}\,(=c_{\text{eff}}^{eeee}) &= c_{11}\cos^4\theta + c_{33}\sin^4\theta + \frac{3}{2}c_{16}\sin^2 2\theta \\
c_{\text{eff}}^{sssf}\,(=c_{\text{eff}}^{eeeo}) &= +/-(c_{23}\sin^2\theta + 3c_{10}\cos^2\theta)\sin\theta \\
c_{\text{eff}}^{ssff}\,(=c_{\text{eff}}^{eeoo}) &= c_{24}\sin^2\theta + c_{18}\cos^2\theta \\
c_{\text{eff}}^{sfff}\,(=c_{\text{eff}}^{eooo}) &= +/-c_{25}\sin\theta \\
c_{\text{eff}}^{ffff}\,(=c_{\text{eff}}^{oooo}) &= c_{22}
\end{aligned}
\tag{8-4}
$$

in the zx plane for (ϕ = 0°/180°, $\Omega_z < \theta < 180° - \Omega_z$), where $c_{\text{eff}}^{sssf} = c_{\text{eff}}^{ssfs} = c_{\text{eff}}^{sfss} = c_{\text{eff}}^{fsss}$, and $c_{\text{eff}}^{ssff} = c_{\text{eff}}^{sfsf} = c_{\text{eff}}^{fssf} = c_{\text{eff}}^{fsfs} = c_{\text{eff}}^{ffss}$, $c_{\text{eff}}^{sfff} = c_{\text{eff}}^{fsff} = c_{\text{eff}}^{ffsf} = c_{\text{eff}}^{fffs}$. The signs of the above equations are compatible with those of Eqs. (6). Note that while the absolute signs are not important for the nonlinear applications, the relative signs among interaction types play a crucial role in a situation where more than one nonlinear processes are optically coupled such as the cascading second-order and direct third-order processes for THG described in this chapter.

3.1 Third-harmonic generation at 0.3547 μm

The THG experiment was carried out in the three principal planes of BIBO by using a Q-switched Nd:YAG laser operating at 1.0642 μm at 10 Hz (Miyata et al., 2008). The 5 × 5 × 5 mm^3 BIBO samples (Fujian Castech Crystal Inc.) used in the experiments were cut at θ = 90°, ϕ = 35.0° in the xy plane, θ = 59.8°, ϕ = +90° (θ = 30.2°, ϕ = −90°) in the yz plane, and θ = 55.3°, ϕ = 0° in the zx planes, respectively, where θ and ϕ are polar and azimuth angles referring to z and x, respectively. The cut angle for the yz plane was obtained at 1.0642 μm at room temperature. A fused silica prism was used to separate the generated TH beam from the other beams.

Type	Plane	Process	PM loci (deg) (θ, ϕ)		$\Delta\theta_{\text{ext}}\cdot\ell$	$\Delta T\cdot\ell$ (°C·cm)	
			Cal.	Exp.	(mrad·cm)	Cal.	Exp.
1	yz	$e_1 + e_1 + e_1 \rightarrow o_3$	(45.6, +/−90)	-	0.44	1.1/0.8	- / -
	zx	$e_1 + e_1 + e_1 \rightarrow o_3$	(67.5, 0)	(67.9, 0)	0.48	2.3	2.1
2	xy	$e_1 + o_1 + o_1 \rightarrow e_3$	(90, 46.7)	(90, 46.7)	1.75[a]	1.3	1.3
	yz	$o_1 + e_1 + e_1 \rightarrow o_3$	(66.4, +/−90)	(66.7, +/−90)	0.83	1.1/0.9	1.2/ -

Table 3. Phase-matching loci and the corresponding angular and temperature acceptance bandwidths (FWHM) for THG at 0.3547 μm in BIBO at 20°C. [a] $\Delta\phi_{\text{ext}}\cdot\ell$ (mrad·cm).

Increasing the input power of the Nd:YAG laser and adjusting the polarization with a retardation plate, the UV signal was easily observed below the damage threshold of this

material. The results for the phase-matching loci and the corresponding temperature bandwidths (FWHM) are tabulated in Table 3 together with the theoretical values calculated by the revised Sellmeier and thermo-optic dispersion formulas presented by Miyata et al. (2009). For the present processes, type-3 interactions are not phase-matchable. Some experimental data in the *yz* plane were not taken because of no effective nonlinearity or no availability of suitable BIBO sample. This table also lists the calculated angular bandwidths, which are used for deriving the temperature bandwidths from the variations of the measured phase-matching angles between 20 and 110 °C. As can be seen, the agreement between theory and experiment is good.

It should be pointed out that in this experiment, unphase-matched SHG at 0.5321 μm was observed with the TH signal, indicating the cascade process involved in the present THG processes. Table 4 lists the magnitude of each cascade process. It is found that there is no direct third-order and cascading second-order contribution to type-1 THG in the *yz* plane. For the other processes, cascading contributions exist and therefore, the observed THG outputs at 0.3547 μm are considered as sum of the direct and cascade processes, as is evident from the observed SHG. From this table, total effective nonlinear constants for the cascade processes are determined to be $\Sigma c_{\mathrm{eff}}^{(2)}$ = 51.1 pm²/V² for type-1 THG in the *zx* plane, and $\Sigma c_{\mathrm{eff}}^{(2)}$ = 12.8 and −30.9/1.4 pm²/V² for type-2 THG in the *xy* and *yz* (ϕ = +90°/−90°) planes, respectively.

Direct cubic process				Cascade process parameters			
Type	Plane	Process	PM loci (deg) (θ, ϕ)	i	Δk_{SHG} (cm^{-1})	$d_{\mathrm{eff}}^{\mathrm{SHG}} d_{\mathrm{eff}}^{\mathrm{SFG}}$ (pm²/V²)	$c_{\mathrm{eff}}^{(2)}$ (pm²/V²)
1	*yz*	$e_1 + e_1 + e_1 \rightarrow o_3$	(45.6, +/−90)	1	–4840	0	0
				2	7065	0	0
	zx	$e_1 + e_1 + e_1 \rightarrow o_3$	(67.9*, 0)	1	–5171	–2.76	32.5
				2	8354	2.39	18.6
2	*xy*	$e_1 + o_1 + o_1 \rightarrow e_3$	(90, 46.7*)	1	–5501	0	0
				2	13450	–7.27	–11.8
				3	–14196	2.45	–6.9
				4	4755	3.43	31.5
	zx	$o_1 + e_1 + e_1 \rightarrow o_3$	(66.7*, +/−90)	1	–5271	0	0
				2	12427	–6.84/1.10	–12.1/2.0
				3	–13314	6.16/0.18	–18.8/–0.6
				4	4384	0	0

Table 4. Cascade process parameters for THG at 0.3547 μm with Δk_{THG}=0 in the principal planes of BIBO at 20°C. * Experimental value.

3.2 Pure $\chi^{(3)}$ third-harmonic generation

Next, 90° phase-matched THG was investigated along the principal axes (Miyata et al., 2009). It is found from Eqs. (5) to (8) that at the propagation direction along *x*, all the second-order susceptibilities vanish whereas all the involved third-order ones remain to be non-zero, indicating the existence of pure cubic processes along this direction, i.e. any cascading quadratic processes are effectively precluded from the nonlinear processes as in the case of

centrosymmetric crystals. In addition, since the large birefringence between n_y and n_z has been found to exist along x, it also indicates the possibility of phase-matching for the pure cubic processes in BIBO. The corresponding effective third-order nonlinear constants for the type-1, type-2, and type-3 processes are expressed as $c_{\text{eff}}^{(3)} = c_{23}$, c_{24}, and c_{25} respectively.

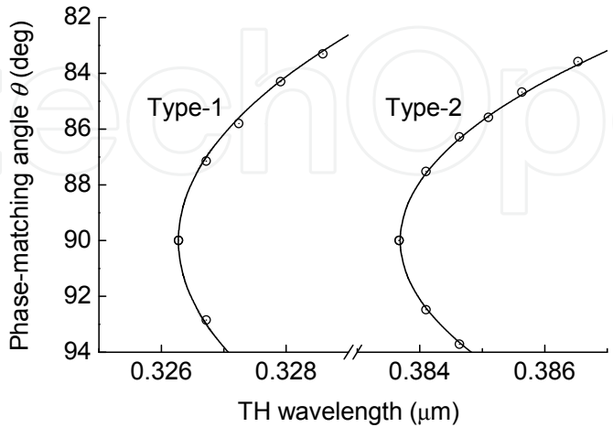

Fig. 1. Phase-matching curves for direct type-1 and type-2 THG in the zx plane of BIBO at 20°C. The circles are our experimental points.

Using the outputs of a KTP OPO pumped by the SH of the same Nd:YAG laser, the phase-matching conditions for the direct type-1 and type-2 THG were checked in the zx plane. Fig. 1 shows the experimental results obtained with a 1.5-cm-long, x-cut BIBO crystal (Crystech Inc.) at 20°C. The solid curve is calculated with the Sellmeier equations and correctly reproduces the experimental points. As can be seen, along the proposed direction x ($\theta = 90^{\circ}$), phase-matched THG was realized at 0.3263 and 0.3837 μm for the type-1 and type-2 interactions, respectively, and no signal of unphase-matched SH was detected, which indicates the absence of possible energy transfer through the SFG ($\omega + 2\omega \rightarrow 3\omega$) process assisted by the non-phase-matched SH, and confirms the generation of the TH purely mediated by cubic nonlinearity.

To investigate further the phase-matching properties for the pure cubic process, the temperature-tuning of phase-matched THG wavelengths was next performed by heating the crystal up to ~120°C with a temperature-controlled copper oven. The experimental points for the type-1 and type-2 processes measured along x of the same sample are plotted in Fig. 2 together with the theoretical curves calculated with the Sellmeier and thermo-optic dispersion formulas. The temperature-tuning rates derived from these experimental points are $d\lambda_{\text{THG}}/dT$ = 0.019 and 0.021 nm/°C for the type-1 and type-2 processes, respectively, which are in excellent agreement with the calculated values of $d\lambda_{\text{THG}}/dT$ = 0.019 and 0.023 nm/°C. For the type-3 process, these formulas predict retracing behaviour and two phase-matching wavelengths of λ_{THG} = 0.5994 and 0.8186 μm with $d\lambda_{\text{THG}}/dT$ = 0.070 and –0.073 nm/°C, respectively. Unfortunately, the experimental verification was precluded because of the limited tunability of the light source. Note that unphase-matched SHG was not observed during the measurement. The phase-matching properties for these pure cubic processes are summarized in Table 5.

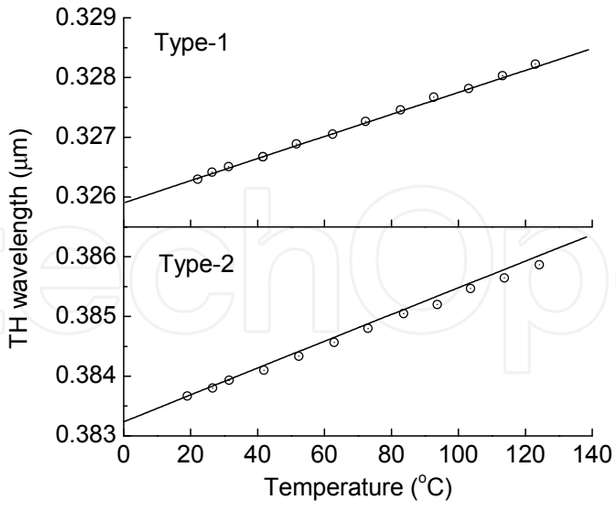

Fig. 2. Temperature-tuned phase-matching curves for direct type-1 and type-2 THG along x of BIBO. The circles are our experimental points.

Type	Process	λ_{THG} (μm)	$\Delta\theta_{ext} \cdot \ell^{1/2}$ (mrad·cm)	$\Delta\phi_{ext} \cdot \ell^{1/2}$ (mrad·cm)	$\Delta\lambda_1 \cdot \ell$ (nm·cm)	$\Delta T \cdot \ell$ (°C·cm)
1	$z_1 + z_1 + z_1 \rightarrow y_3$	0.3263*	1.96	3.77	0.08	1.4*
2	$y_1 + z_1 + z_1 \rightarrow y_3$	0.3837*	2.55	4.98	0.20	3.1*
3	$y_1 + y_1 + z_1 \rightarrow y_3$	0.5994	4.45	8.70	3.11	14.9
		0.8186	5.28	10.13	6.01	27.6

Table 5. Phase-matched pure $\chi^{(3)}$ THG wavelengths and the corresponding angular, spectral, and temperature acceptance bandwidths (FWHM) along x of BIBO at 20°C. * Experimental value.

3.3 Three-photon downconversion

From the results given in the preceding, phase-matching interactions for the other types of pure cubic processes are expected to be obtained along the x axis. Here, we consider the three-photon downconversion processes ($\omega_a + \omega_b + \omega_c = \omega_p$). Fig. 3 shows the corresponding phase-matching curves for the type-1 interaction at 20°C. As can be seen, the spectral range of the pump beam is somewhat limited, which is attributed to the UV transmission cutoff wavelength of ~ 0.270 μm (Teng et al., 2001) and the symmetrical relations of the curves among three down-converted waves. The longest pump wavelength is fixed at 0.9789 μm, corresponding to the phase-matched fundamental wavelength for type-1 THG.

In contrast, the tuning curves for the type-2 and type-3 processes give asymmetry relations, resulting in the wide spectral range of the pump beam, as shown in Fig. 4. Thus, for example, using the Nd:YAG laser at 1.0642 μm as the fundamental source in the system, it is possible to pump with the SH (λ_p = 0.5321 μm) or TH (λ_p = 0.3547 μm) beams for the type-2 process, and with the fundamental, SH, or TH beams for the type-3 process. Similarly, the Ti:sapphire laser can be also used as the fundamental source for these processes.

It should be pointed out that at the given pump wavelength, the tuning curves cover the very broad spectral ranges of down-converted waves, except the vicinity of the three-wavelength

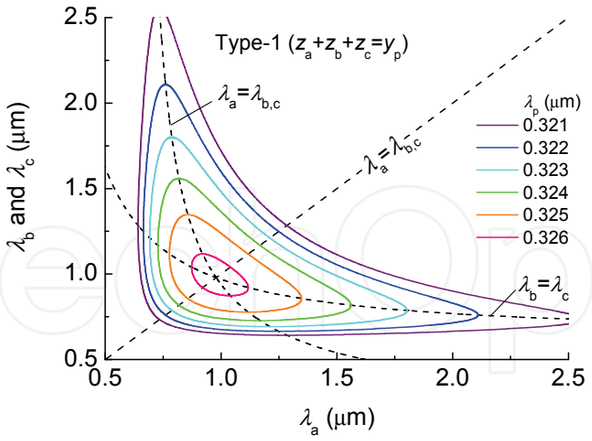

Fig. 3. 90° phase-matching curves for type-1 downconversion processes ($\omega_a + \omega_b + \omega_c = \omega_p$) along x of BIBO at 20°C. The crossing point of the dashed curves corresponds to the degeneracy point.

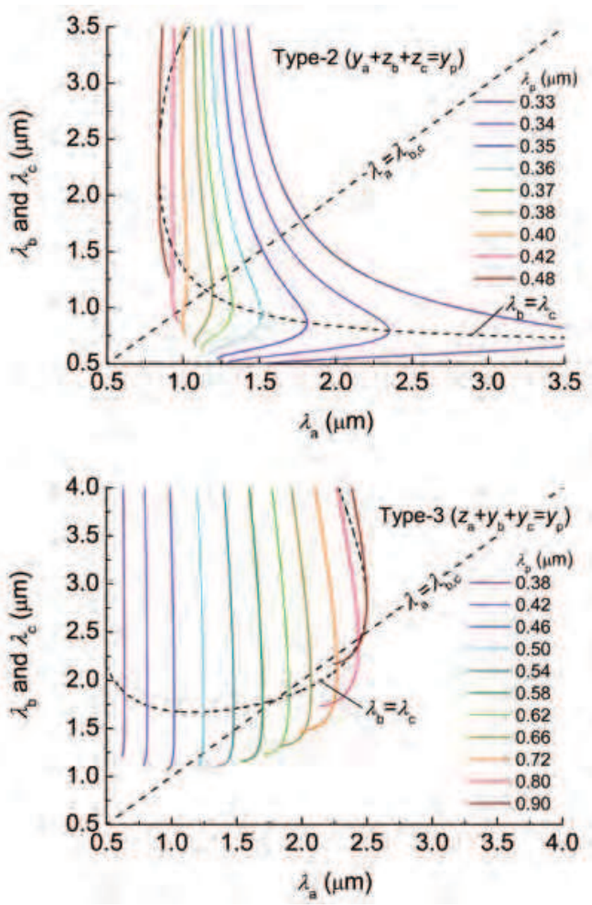

Fig. 4. 90° phase-matching curves for type-2 and type-3 downconversion processes ($\omega_a + \omega_b + \omega_c = \omega_p$) along x of BIBO at 20°C. The crossing point of the dashed curves corresponds to the degeneracy point.

degeneracy point ($\lambda_a = \lambda_b = \lambda_c = 3\lambda_p$) for the type-1 process. This indicates the possibility of unltrabroadband pulse generation with the proper selection of the wavelength of the seed beam. Especially, the interesting points are located at the two-wavelength degeneracy points that are shown with the dashed curves in the figures. It is found that in contrast to the second-order process, two-wavelength degeneracy points are generally obtained at the given crystal orientation and pump wavelength for the third-order processes.

4. Discussion

Recently, some attempts for reducing the cascading quadratic contribution in noncentrosymmetric crystals have been made by Boulanger and co-workers. Their motivation is the quantum properties of three photons that are created by direct cubic downconversion process (Felbinger et al., 1998). They have stated that the cascading quadratic processes are detrimental factor in the quantum correlation experiments based on the cubic nonlinearity, because of the different quantum properties of cascade and direct processes. With the low cascading contribution relative to the direct cubic process, i.e. $[\chi^{(2)}:\chi^{(2)}/\chi^{(3)}]^2 = 10\%$ (Boulanger et al., 1999), they have obtained the efficient THG along the propagation direction x of KTP (Feve et al., 2000). Their further research has led to the nearly pure cubic difference-frequency generation with $[\chi^{(2)}:\chi^{(2)}/\chi^{(3)}]^2 = 0.5\%$ in the same material (Douady & Boulanger, 2004, 2005), which is attributed to the relative sign and amount of the phase-mismatching factor for each non-zero second-order process (see Eqs. (3) and (4)). However, this approach gives the pure $\chi^{(3)}$ condition only for a specific frequency- conversion process either with a specific phase-matching configuration (Douady & Boulanger, 2005) or with the help of periodical poling to the material (Feve & Boulanger, 2002).

In this study, pure $\chi^{(3)}$ THG was realized along x of BIBO. The proposed condition, which simultaneously satisfies the two requirements, (1) nonlinear optical coupling of zero second-order and non-zero third-order processes and (2) birefringence property, was given as a result of the symmetry operation of two-fold rotation axis. Provided that the corresponding cubic nonlinearity doesn't vanish owing to the symmetry operations of the other symmetry elements, any frequency-conversion schemes are considered to be purely cubic for propagation along the two-fold rotation axis. It is clear that this is equivalent to using a non-zero cubic interaction in a centrosymmetric crystal under the 90° phase-matching condition, as was demonstrated in TiO_2 rutile by Gravier and Boulanger (2006, 2007) for the direct type-2 THG.

Finally, note that third-order frequency downconversions have been also achieved in centrosymmetric CaF_2 and BaF_2 with non-collinear geometry for widely tunable, ultrashort-pulse IR generation. (Okamoto & Tasumi, 1995; Nienhuys et al., 2001). Their phase-matching conditions in the transparent range can be fulfilled only by four-wave mixing, $\omega_1 + \omega_2 = \omega_3 + \omega_4$, owing to the absence of birefringence property. Regardless of the presence of inversion centre, the birefringence requirement of phase-matching for the present third-order processes, $\omega_1 + \omega_2 + \omega_3 = \omega_4$, does not allow the use of isotropic crystals and an optic axis direction of anisotropic crystals without manipulation of the material structure. Consequently, it is found from the symmetry requirements that with the suitable birefringence, the pure cubic process under the phase-matching condition, $k_1 + k_2 + k_3 - k_4 = 0$ ($k > 0$), can be attained in nine and eight point symmetry classes of centrosymmetric and noncentrosymmetric crystals, respectively (see Table 6), while for the latter, the approach proposed by Douady and Boulanger (2005) may give additional material choices without restriction of symmetry.

stem	Point symmetry	
	Centrosymmetric	Noncentrosymmetric
Triclinic	$\bar{1}$	-
Monoclinic	$2/m$	2
Orthorhombic	mmm	$222, mm2$
Tetragonal	$4/m, 4/mmm$	$422, \bar{4}2m$
Trigonal	$\bar{3}, \bar{3}m$	32
Hexagonal	$6/m, 6/mmm$	$622, \bar{6}m2$

Table 6. Point symmetry classes of centrosymmetric and non-centrosymmetric, non-cubic crystals with zero second-order and nonzero third-order nonlinearities.

5. Conclusion

Because of the multi-photon interactions, numerous interesting applications can be found for higher-order processes. While the cascade process of the lower-order nonlinearity interferes with the direct process in noncentrosymmetric media, its magnitudes can be controlled by the phase-mismatching factor and effective nonlinear constants, and it can be a beneficial or harmful effect, depending on the purpose. Enhancement of the cascade process provides high conversion efficiency in the overall process, whereas its suppression or its separation from the direct process becomes important whenever the quantum properties for higher-order processes are investigated.

This study revealed that even under no inversion symmetry, phase-matched pure $\chi^{(3)}$ THG can be obtained along the two-fold rotation axis, and other pure cubic interactions expressed by $\omega_1 + \omega_2 + \omega_3 = \omega_4$ are also possible at the same propagation direction, with the suitable birefirengence. This new result in nonlinear optics is important not only from the fundamental point of view, but also for its practical applications to the measurements on the nonlinear susceptibilities and quantum properties for higher-order processes in noncentrosymmetric media.

6. References

Akhmanov S. A.; Duvobic A. N.; Saltiel S. M.; Tomov I. V. & Tunkin V. G. (1974). Nonlinear optical effects of fourth order in the field in a lithium formate crystal, *JETP Lett.*, Vol. 20, pp. 117-118.

Akhmanov S. A.; Martynov X. A.; Saltiel S. M.; & V. G. Tunkin (1975). Observation of nonresonant six-photon processes in a calcite crystal, *JETP Lett.,* Vol. 22, pp. 65-67.

Banks P. S.; Feit M. D.; & Perry M. D. (1999). High-intensity third-harmonic generation in beta barium borate through second-order and third-order susceptibilities, *Opt. Lett.*, Vol. 24, pp. 4-6.

Banks P. S.; Feit M. D. & Perry M. D. (2002). High-intensity third-harmonic generation, *J. Opt. Soc. Am. B*, Vol. 19, pp. 102-118.

Boulanger B.; Feve J. P.; Delarue P.; Rousseau I. & Marnier G. (1999). Cubic optical nonlinearity of $KTiOPO_4$, *J. Phys. B: Atm. Mol. Opt. Phys.,* Vol. 32, pp. 475-488.

Chemla D. S.; Begley R. F.; & R. L. Byer (1974). Experimental and theoretical studies of third-harmonic generation in the chalcopyrite $CdGeAs_2$, *IEEE J. Quantum Electron.* QE-10, pp. 71-81.

Douady J. & Boulanger B. (2004). Experimental demonstration of a pure third-order optical parametric downconversion process, *Opt. Lett.* Vol. 29, pp. 2794-2796.

Douady J. & Boulanger B. (2005). Calculation of quadratic cascading contributions associated with a phase-matched cubic frequency difference generation in a $KTiOPO_4$ crystal, *J. Opt. A: Pure and Applied Optics,* Vol. 7, pp. 467-471.

Feve J. P.; Boulanger B. & Guillien Y. (2000). Efficient energy conversion for cubic third-harmonic generation that is phase matched in $KTiOPO_4$, *Opt. Lett.* Vol. 25, pp. 1373-1375.

Feve J. P. & Boulanger B. (2002). Suppression of quadratic cascading in four-photon interactions using periodically poled media, *Phys. Rev. A*, Vol. 65, pp. 063814-063814-6.

Felbinger T.; Schiller S. & Mlynek J. (1998). Oscillation and generation of nonclassical states in three-photon down-conversion, *Phy. Rev. Lett.*, Vol. 80, pp. 492-495.

Gravier F. & Boulanger B. (2006). Cubic parametric frequency generation in rutile single crystal, *Opt. Express*, Vol. 14, pp. 11715-11720.

Gravier F. & Boulanger B. (2007). Third order frequency generation in TiO_2 rutile and $KTiOPO_4$, *Opt. Mater.*, Vol. 30, pp. 33-36.

Hellwig H.; Liebertz J. & Bohaty L. (1999). Exceptional large nonlinear optical coefficients in the monoclinic bismuth borate BiB_3O_6 (BIBO), *Solid State Commun.,* Vol. 109, pp. 249-251.

Hellwig H.; Liebertz J.; & Bohaty L. (2000). Linear optical properties of the monoclinic bismuth borate BiB_3O_6, *J. Appl. Phys.,* Vol. 88, pp. 240-244.

Kildal H. & Iseler G. W. (1979). Higher-order nonlinear processes in $CdGeAs_2$, *Phys. Rev. B* Vol. 19, pp. 5218-5222.

Miller S.; Rotermund F.; Xu G.; Noack F.; Panyutin V. & Petrov V. (2008). Polarization-dependent nonlinear refractive index of BiB_3O_6, *Opt. Mater.*, Vol. 30, pp. 1469-1472.

Miyata K.; Mikami T.; Umemura N. & Kato K. (2008). Direct third-harmonic generation in BiB_3O_6, *Proceedings of SPIE*, Vol. 6875, 687518-687518-5.

Miyata K.; Umemura N. & K. Kato (2009). Phase-matched pure $\chi^{(3)}$ third-harmonic generation in noncentrosymmetric BiB_3O_6, *Opt. Lett.,* Vol. 34, 500-502.

Nienhuys H. K.; Planken P. C. M.; Santen R. A. V. & Bakker H. J. (2001). Generation of mid-infrared generation in CaF_2 and BaF_2, *Opt. Lett.*, Vol. 26, pp. 1350-1352.

Okada M. (1971). Third-order nonlinear optical coefficients of $LiIO_3$, *Appl. Phys. Lett.,* Vol. 18, pp. 451-452.

Okamoto H. & Tasumi M. (1995). Generation of ultrashort light pulses in the mid-infrared (3000–800 cm^{-1}) by four-wave mixing, *Opt. Commun.*, Vol. 121, pp. 63-68.

Penzkofer A.; Ossig F.; & P. Qiu (1988). Picosecond third-harmonic light generation in calcite, *Appl. Phys. B*, Vol. 47, pp. 71-81.

Qiu P. & Penzkofer A. (1988). Picosecond third-harmonic light generation in β-BaB_2O_4, *Appl. Phys. B,* Vol. 45, pp. 225-236.

Takagi Y. & Muraki S. (2000). Third-harmonic generation in a noncentrosymmetrical crystal: direct third-order or cascaded second-order process?, *J. Luminesc.,* Vol. 87-89, pp. 865-867.

Teng B.; Wang J.; Wang Z.; Jiang H.; Hu X.; Song R.; Liu H.; Liu Y.; Wei J. & Shao Z. (2001). Growth and investigation of a new nonlinear optical crystal: bismuth borate BiB_3O_6, J. Cryst. Growth, Vol. 224, pp. 280-283.

Terhune R. W.; Maker P. D.; & Savage C. M. (1962). Optical harmonic generation in calcite, *Phys. Rev. Lett.*, Vol. 62, pp. 404-406.

Terhune R. W.; Maker P. D. & Savage C. M. (1963). Observation of saturation effects in optical harmonic generation, *Appl. Phys. Lett.*, Vol. 2, pp. 54-55.

Tzankov P. & Petrov V. (2005). Effective second-order nonlinearity in acentric optical crystals with low symmetry, *Appl. Opt.*, Vol. 44, 6971-6985.

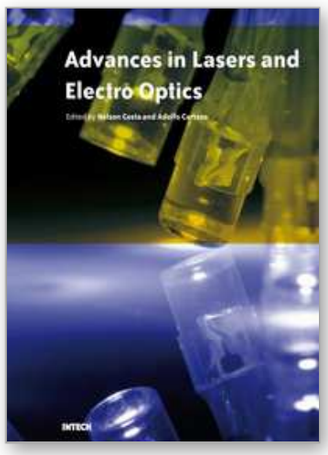

Advances in Lasers and Electro Optics

Edited by Nelson Costa and Adolfo Cartaxo

ISBN 978-953-307-088-9
Hard cover, 838 pages
Publisher InTech
Published online 01, April, 2010
Published in print edition April, 2010

Lasers and electro-optics is a field of research leading to constant breakthroughs. Indeed, tremendous advances have occurred in optical components and systems since the invention of laser in the late 50s, with applications in almost every imaginable field of science including control, astronomy, medicine, communications, measurements, etc. If we focus on lasers, for example, we find applications in quite different areas. We find lasers, for instance, in industry, emitting power level of several tens of kilowatts for welding and cutting; in medical applications, emitting power levels from few milliwatt to tens of Watt for various types of surgeries; and in optical fibre telecommunication systems, emitting power levels of the order of one milliwatt. This book is divided in four sections. The book presents several physical effects and properties of materials used in lasers and electro-optics in the first chapter and, in the three remaining chapters, applications of lasers and electro-optics in three different areas are presented.

InTech Europe
University Campus STeP Ri
Slavka Krautzeka 83/A
51000 Rijeka, Croatia
Phone: +385 (51) 770 447
Fax: +385 (51) 686 166
www.intechopen.com

InTech China
Unit 405, Office Block, Hotel Equatorial Shanghai
No.65, Yan An Road (West), Shanghai, 200040, China
中国上海市延安西路65号上海国际贵都大饭店办公楼405单元
Phone: +86-21-62489820
Fax: +86-21-62489821

IntechOpen